J Neuropathol Exp Neurol
Vol. 65, No. 10
October 2006
pp. 976–987

ORIGINAL ARTICLE

Plaque-Associated Overexpression of Insulin-Degrading Enzyme in the Cerebral Cortex of Aged Transgenic Tg2576 Mice With Alzheimer Pathology

María C. Leal, MS, Verónica B. Dorfman, PhD, Agata Fernández Gamba, MS, Blas Frangione, MD, PhD, Thomas Wisniewski, MD, Eduardo M. Castaño, MD, Einar M. Sigurdsson, PhD, and Laura Morelli, PhD

Abstract

It was proposed that insulin-degrading enzyme (IDE) participates in the clearance of amyloid β (Aβ) in the brain, and its low expression or activity may be relevant for the progression of Alzheimer disease. We performed a longitudinal study of brain level, activity, and distribution of IDE in transgenic mice (Tg2576) expressing the Swedish mutation in human Aβ precursor protein. At 16 months of age, Tg2576 showed a significant 2-fold increment in IDE protein level as compared with 4.5- and 11-month-old animals. The peak of IDE was in synchrony with the sharp accumulation of sodium dodecyl sulfate-soluble Aβ and massive Aβ deposition into plaques. At this stage, IDE appeared surrounding Aβ fibrillar deposits within glial fibrillar acidic protein-positive astrocytes, suggesting that it was locally overexpressed during the Aβ-mediated inflammation process. When primary astrocytes were exposed to fibrillar Aβ in vitro, IDE protein level increased as compared with control, and this effect was reduced by the addition of U0126, a specific inhibitor of the ERK1/2 mitogen-activated protein kinase cascade. We propose that in Tg2576 mice and in contrast to its behavior in Alzheimer brains, active IDE increases with age around plaques as a component of astrocyte activation as a result of Aβ-triggered inflammation.

Key Words: Alzheimer disease, Amyloid β, Astrocytes, Inflammation, Insulin-degrading enzyme, Microglia, MAPK cascades, Transgenic mice.

INTRODUCTION

One of the pathologic features of Alzheimer disease (AD) brain is the presence of senile plaques in the cerebral cortex composed of amyloid β (Aβ) peptide, dystrophic neurites, neurofibrillary tangles, and congophilic angiopathy (1). In patients with sporadic AD, the accumulation of Aβ in the diseased brain is a complex and heterogeneous process (2) involving secretase activity (3), impaired clearance or deficient peptide catabolism, or both (4, 5). In this context, proteolytic processing of Aβ deserves special attention because it is one of the major factors that modulates the levels of brain-soluble Aβ. A group of zinc–metalloendopeptidases, including Neprilysin, endothelin-converting enzymes, and insulin-degrading enzyme (IDE), may regulate the steady state levels of Aβ in the mammalian brain. The physiological role of these proteases in vivo has been recently confirmed with functional studies using genetic deletion strategies in mice ([6–9], reviewed in [10]). Moreover, transgenic overexpression of IDE and Neprilysin in a mouse model of AD showed a dramatic decrease in brain Aβ levels and prolonged lifespan (11, 12). IDE, or insulysin (13), is a ubiquitous metalloendopeptidase capable of degrading several peptides with a high propensity to form amyloid fibrils in vitro and in vivo. These include insulin, glucagon, amylin, atrial natriuretic peptide, calcitonin, Aβ ([14], reviewed in [15]), and the ABri and ADan peptides associated with hereditary dementia (16). IDE knockout mice showed accumulation of the carboxyl terminal intracellular domain of APP, hyperinsulinemia, and increased Aβ brain levels with an inverse correlation with IDE activity among homozygous, heterozygous, and wild-type mice for the insulysin gene trap model (7–9). The IDE gene, located in chromosome 10q23.3, has been linked to type 2 diabetes (17, 18) and is close to a region of linkage for late-onset AD, representing a positional and biologic candidate for late-onset AD susceptibility (19). To date, no mutations have been found in the canonic isoform of IDE and the recent haplotype association studies have produced inconsistent results (20–24). Despite these controversial genetic data, the biochemical and functional findings suggest that IDE may participate in the pathogenesis of sporadic late-onset AD (7, 9, 19, 25, 26). The recent advances in our knowledge on Aβ degradation raise the possibility that brain proteases may be

From the Fundación Instituto Leloir (MCL, VBD, AFG, EMC, LM), Instituto de Investigaciones Bioquímicas de Buenos Aires (CONICET), Ciudad de Buenos Aires, Argentina; and the Departments of Psychiatry (BF, TW, EMS), Pathology (TW), and Neurology (BF, TW, EMS), New York University School of Medicine, New York, NY.
Send correspondence and reprint requests to: Laura Morelli, PhD, Fundación Instituto Leloir-Instituto de Investigaciones Bioquímicas de Buenos Aires (CONICET). Patricias Argentinas 435, Ciudad de Buenos Aires C1405BWE, Argentina; E-mail: lmorelli@leloir.org.ar
This work was supported by grants from the Alzheimer's Association IIRG 03-5312, Agencia Nacional de Promoción Científica y Tecnológica-PICT 05-10599, and NIH grants AG020197, AG05891, and AG020245.
Figures 4–6 can be viewed online in color on www.jneuropath.com.

manipulated to promote Aβ clearance. To facilitate these efforts, several aspects related to endogenous IDE expression, subcellular localization, and activity need to be carefully addressed in animal models of AD. The specific aim of our work was to study the profile of endogenous IDE during the neurodegenerative process in transgenic mice (Tg2576) brains, which carry the human amyloid precursor protein gene with the "Swedish" double mutation associated with familial AD (APPsw) and robustly recapitulate the neuropathology of AD (27). Early and late, temporal, and spatial characteristics of IDE expression were studied in Tg2576 mice at 4.5, 11, and 16 months of age. We found that aged Tg2576 mice showed a 2-fold increment in IDE protein levels as compared with 11 month olds, whereas no differences were found in the amount of IDE transcripts in whole brain homogenates, suggesting that the regulation of IDE gene expression in aged mice may occur at the posttranscription level. Moreover, at this stage, IDE appeared surrounding amyloid deposits within glial fibrillar acidic protein (GFAP)-positive astrocytes, suggesting that IDE was focally expressed by cells involved in the inflammatory response. Results from our in vitro experiments fully support the hypothesis that IDE expression is mediated by an inflammatory process involving mitogen-activated protein kinase (MAPK) signaling. The finding that Aβ deposition in aged Tg2576 mice is related to IDE overexpression at late stages of the neuropathologic process in this animal model of AD raises the possibility of a new role of IDE independent of its proteolytic activity in the process of amyloid deposition in the brain.

MATERIALS AND METHODS

Animals

Hemizygous Tg2576 mice (27) and nontransgenic strain littermates (NTg) were maintained on a 12-hour light/dark cycle and standard diet. Animal care was in accordance with an approved protocol following the institutional guidelines at New York University School of Medicine. A total of 32 animals were divided into 6 experimental groups as follows (number of animals and mean age ± standard error of mean in parentheses): group 1: Tg2576 (n = 6; 4.92 ± 0.15 months); group 2: NTg (n = 6; 4.75 ± 0.11 months); group 3: Tg2576 (n = 4; 11.75 ± 0.48 months); group 4: NTg (n = 6; 10.75 ± 0.40 months); group 5: Tg2576 (n = 5; 16.3 ± 0.44 months); and group 6: NTg (n = 5; 15.8 ± 0.2 months).

Tissue Preparation

Mice were anesthetized with sodium pentobarbital (150 mg/kg intraperitoneally), perfused transaortically with sodium phosphate buffer, pH 7.4, and the brains (free of cerebellum and medulla) processed as described previously (28). The right hemisphere was fixed overnight by immersion in a periodate–lysine–paraformaldehyde solution, subsequently transferred to phosphate-buffered saline (PBS) containing 20% glycerol and 2% dimethyl sulfoxide (DMSO), and stored at 4°C until sectioned. The left hemisphere was snap-frozen in liquid nitrogen for protein and RNA extraction. As a result of limitations imposed by the limited number of Tg2576 animals and the amount of material required for various biochemical procedures, whole brain homogenates were prepared instead of homogenates from isolated cerebral cortex.

Antibodies

Rabbit polyclonal BC2 antiserum was generated against a glutathione S-transferase (GST) fusion protein containing the sequence 97–273 of rat IDE as described previously (29). Anti-GST polyclonal antibodies were affinity purified using glutathione-(oxidized)–agarose beads (Sigma, St. Louis, MO). Anti-IDE monoclonal antibodies were obtained by immunization of Balb/c mice with full-length recombinant IDE (rIDE) following standard protocols. Anti-rIDE clones 1C1 and 3A2 (isotype IgG1) that did not recognize GST-IDE97-273 by direct enzyme-linked immunosorbent assay (ELISA) were further characterized using GST fusion proteins spanning 3 different regions of IDE: R1, amino acids 42–186; R3, 262–530; and R4, 531–998, respectively. To obtain greater amounts of antibodies, selected clones were propagated in vivo by the production of ascitic fluid and purified according to standard protocols. Monoclonal anti-α actin was from Sigma. Rabbit polyclonal antineuronal specific enolase (NSE) and anti-GFAP were obtained from Santa Cruz Biotechnology (Santa Cruz, CA) and DAKO (Glostrup, Denmark), respectively. Monoclonal anti-flotillin 1 was from BD Transduction Laboratories, Inc. (Mountain View, CA). Monoclonal antibody IgG1 anti-β lactamase was provided by Dr. J. Santos from the University of Buenos Aires. Polyclonals anti-p38, antiphosphorylated p38, anti-ERK2, and monoclonal anti-phospho ERK1/2 (p-ERK1 p44/p-ERK2 p42) were from Santa Cruz Biotechnology. Biotinylated goat anti-mouse IgG was from Vector Laboratories (Burlingame, CA). Cy5-streptavidin and Cy3-goat anti-rabbit IgG were from Amersham Biosciences (Buckinghamshire, U.K.).

Chemicals

Protein inhibitors phenylmethyl sulfonyl fluoride (PMSF), pepstatin, leupeptin, EDTA, and aprotinin as well as MAPK inhibitor U0126 (1,4-diamino-2,3-dicyano-1,4 bis[2-aminophenylthio]butadiene) were from Sigma. Protein G-Sepharose was from Amersham Biosciences.

Protein Extraction Protocols

Portions of 50 to 70 mg of each frozen hemibrain were homogenized with a manual Teflon glass homogenizer in 1 mL of ice-cold PBS containing 1 mM PMSF, 5 μg/mL pepstatin A, 5 μg/mL leupeptin, and 5 μg/mL aprotinin. The homogenates were centrifuged at 100,000 × *g* at 4°C for 1 hour using a Beckman ultracentrifuge and a 50Ti rotor (Beckman, Palo Alto, CA). Supernatants corresponding to water-soluble brain fractions were aliquoted and stored at −80°C. Pellets were exhaustively washed in 0.5 M Na_2CO_3 pH 11 to disrupt weak protein–protein associations and subjected to protein extraction using 2% sodium dodecyl sulfate (SDS) by homogenization and posterior centrifugation at 100,000 × *g* at 4°C for 1 hour. SDS-soluble fractions were aliquoted and stored as described. Individual samples from each extraction step were grouped by

transgene status and age. Six different pools—from each extraction protocol—corresponding to Tg2576 and control littermates were analyzed to assess IDE levels and activity. These were normalized by protein content as determined with a bicinchoninic acid assay (Pierce, Rockford, IL).

Immunoblotting

For Western blotting, aliquots of 10 to 50 μg of proteins were subjected to electrophoresis on 7.5% SDS-Tris-Tricine polyacrylamide minigels and transferred to polyvinylidene fluoride (PVDF) membranes (Amersham Biosciences). After blocking overnight with 5% nonfat dry milk–PBS, membranes were probed with the primary antibodies in PBS containing 0.1% Tween 20 followed by horseradish peroxidase–conjugated antigammaglobulin (Amersham Biosciences). For visualization, blots were incubated with ECL Plus (Amersham Biosciences), scanned in a STORM 840, and processed using the computer software ImageQuant (Amersham Biosciences).

Insulin-Degrading Enzyme and Aβ Quantitation by Enzyme-Linked Immunosorbent Assay

Aβ40 and Aβ42 levels were assessed using a sandwich ELISA system commercially available (Signet Labs, Dedham, MA) and results expressed as ng/mg of tissue protein. IDE was quantified by a sandwich ELISA using monoclonal antibodies 3A2 and biotinylated 1C1 as previously described (30). Levels of endogenous IDE were expressed as ng/mg of tissue protein. Determinations were performed in duplicate samples in 2 independent experiments for Aβ and in 4 independent experiments for IDE, respectively.

Insulin-Degrading Enzyme Immunoprecipitation and Activity Assay

To assess the activity of endogenous IDE, we followed a previously described protocol (30) with slight modifications as follows. Two hundred fifty micrograms of proteins from a PBS high-speed supernatant from brain homogenates was diluted in 500 μL of PBS, pH 7.5, containing 2 mM PMSF, 2 μg/mL leupeptin, 2 μg/mL aprotinin, and 2 μg/mL pepstatin A and incubated with 9 μg of each anti-IDE monoclonal antibodies 1C1 and 3A2 or anti-α-actin monoclonal antibody as control, respectively, and protein G-Sepharose for 3 hours at room temperature. Immunocomplexes were washed 3 times in ice-cold PBS containing 0.4 M NaCl and 3 times in 0.1 M phosphate, pH 7 (degradation buffer) without protein inhibitors. The protein G-Sepharose beads were then incubated in 50 μL of degradation buffer containing 50,000 cpm of ^{125}I-insulin (specific activity, 300 μCi/μg; provided by Edgardo Poskus, University of Buenos Aires) for the indicated times at 37°C with constant agitation in the presence or absence of the following protease inhibitors: 5 mM EDTA, 1 mM 1,10-phenanthroline, 2 mM PMSF, 2 μg/mL leupeptin, 2 μg/mL pepstatin A, and 2 μg/mL aprotinin. After incubation, Sepharose beads were centrifuged at 1,500 × *g* for 5 minutes. Twenty microliters of the supernatant were removed, mixed with an equal volume of 8% SDS sample buffer, boiled, and resolved by 15% Tris-Tricine SDS-PAGE under nonreducing conditions. The amount of intact remaining ^{125}I-insulin was estimated with a Storm 840 PhosphorImager and proteolysis expressed as the percentage of degradation determined by $(A/B) \times 100$ where *A* represents the intensity of intact ^{125}I-insulin after the incubation with anti-IDE immunoprecipitates from mouse brain homogenates and *B* the intensity of intact ^{125}I-insulin after the immunoprecipitation (under identical experimental conditions) of 500 ng of rIDE.

Mouse Brain Insulin-Degrading Enzyme mRNA Quantification by Competitive Reverse Transcriptase–Polymerase Chain Reaction

Total RNA was extracted from 40 to 60 mg of frozen hemibrain tissue using RNeasy lipid tissue kit (Qiagen, Hilden, Germany). Traces of DNA were removed by treatment with RNase-free DNase I (Qiagen). Individual samples were grouped by transgene status and age. RNA integrity was assessed by reverse transcriptase–polymerase chain reaction (RT-PCR) of endogenous glyceraldehyde-3-phosphate dehydrogenase (GPDH) using the following set of primers: forward, 5′-TCCCTCAAgATTgTCAgCAA-3′; reverse, 5′-AATCCACAACggATACATT-3′. Competitor cDNA homologous to the catalytic site of IDE located in exon 3 was obtained as follows. Two sets of primers: 304, 5′-CCggATCCCTgTCAgACCCTCCA-3′; NT, 5′-AAACTggCTgTATTCATTTTCCTT-3′, and CT, 5′-gCATTTACCAgCggAgAACACACC-3′; 573C, 5′-TCgAATTCgACAgCGTTCACCTC-3′ were used to amplify fragments called NT (102 bp) and CT (141 bp), respectively, from pCDNA3-IDE containing the coding region of rat IDE cDNA. After NT-CT ligation and subcloning into pGEM-T Easy vector (Promega. Madison, WI), a fragment of 259 bp was obtained. Competitor RNA was prepared using the RT-PCR Competitor Construction Kit (Ambion, Austin, TX) and quantified following the manufacturer's instructions. Both cDNA from endogenous mRNA and competitor RNA were prepared by reverse transcription of 0.5 μg of tissue RNA in the presence of a known amount of competitor RNA following standard protocols. Final PCR products were separated on 8.4% polyacrylamide gels, stained with ethidium bromide solution, visualized under an ultraviolet transilluminator (UVP Life Sciences, Cambridge, U.K.), and bands of 285 bp and 259 bp were quantified using Media Cybernetics Gel-Pro Analyzer software (version 3.1; Silver Spring, MD). The ratio of products obtained from the endogenous and exogenous targets at the end of the amplification reflects the initial ratio of endogenous target to the competitor. Three independent experiments were performed and results were expressed as copies of competitor mRNA/μg of sample mRNA.

Immunohistochemistry

Serial coronal 40-μm free-floating sections were stored in sucrose–ethylenglycol–PBS solution at −20°C until assayed. Retrieval of antigen sites, blocking of endogenous peroxidase activity, and blocking of nonspecific binding sites was performed according to standard protocols. A mouse-on-mouse immunodetection kit from Vector Laboratories

(Burlingame, CA) was used for immunolocalization of IDE with purified monoclonal antibodies 1C1/3A2 at 0.5 μg/μL. Nonspecific immunohistochemical controls for anti-IDE included the omission of the primary antibody, the incubation of an adjacent section with 1 μg/μL of 1C1/3A2 in the presence of 5 μg/μL of rIDE, or with an unrelated antibody-purified mouse IgG1 monoclonal antibody anti-*B. lichen-iformis* exo small β-lactamase (31). Immunoreactivity was developed using 3,3-diaminobenzidine tetrahydrochloride (DAB) substrate with nickel ammonium sulfate intensification (Vector Laboratories). To visualize fibrillar Aβ deposits, sections were stained with 1% Thioflavine-S (Sigma) for 10 minutes and examined with a fluorescence microscopy as described subsequently. Double immunostaining of IDE and fibrillar deposits was assessed using 1C1/3A2 and thioflavin-S. For localization of IDE in activated astrocytes, we used a mix of 1C1/3A2 and anti-GFAP as primary antibodies. Specific immunoreactivity was visualized in a confocal microscopy (as described subsequently) with biotinylated goat anti-mouse IgG conjugated to Cy5-streptoavidin (blue fluorescence for IDE detected using helio/neon 633-nm laser) and Cy3-labeled goat anti-rabbit IgG (red fluorescence for GFAP detected using helio/neon 543-nm laser). To colocalize IDE in microglial cells, 1C1/3A2 immunoreactivity was detected as described previously and sections were further incubated with fluorescein isothiocyanate (FITC)-*Lycopersicum esculentum* (tomato) lectin (Sigma) overnight at 4°C and viewed under an argon 488-nm laser. Analysis of the images was performed as described subsequently.

Astrocyte Cultures and Treatments

Primary astrocytes were obtained from the cerebral cortex of 1- to 2-day-old neonatal Sprague-Dawley rats freed of meninges following protocols previously described (32) and kept in culture until confluency by addition of culture medium containing DMEM and Ham's F12 (1:1 v/v), 5 μg/mL streptomycin, 5 U/mL penicillin, and supplemented with 10% fetal bovine serum (Gibco, Carlsbad, CA). For immunocytochemistry, cells were detached with 0.25% trypsin and plated at 0.5 to 1.5 $\times$ 10^5 cells/well onto 8-well Lab-TeK chamber slide (Nunc, Naperville, IL). To obtain fibrillar Aβ, synthetic Aβ1-40 peptide (Bachem, Torrance, CA) was dissolved in DMSO to 250 μM, stored at -20°C for at least 4 weeks, and diluted to 5 μM in cell culture media just before use. After this procedure, Aβ solution contained predominantly fibrils when characterized by electron microscopy. Disaggregated (referred to as soluble) peptide was obtained by dissolving lyophilized peptide in 1,1,1,3,3,3-hexafluoro-2-propanol (HFIP) and following the protocol as previously described (33). Because fibrillar Aβ mediates inflammation by MAPK cascades, we tested its capability to induce astroglial IDE expression through ERK1/2 phosphorylation. Specificity of the effect was confirmed by inhibition of ERK1/2 with 50 μM of U0126. Stimulation with fibrillar Aβ was performed in 2 sets of plates containing cells cultured in serum-free media for 24 hours in the presence or absence of MAPK inhibitor (added 1 hour before stimulation). After 1 hour, one set was processed to test the levels of p-ERK1/2 (peak of kinase activation) and the other one was incubated overnight to quantify IDE expression. For immunolocalization of IDE, cells were fixed with p-formaldehyde, permeabilized with 0.1% Triton X-100, and blocked with 5% normal goat serum as previously described (30). Slides were probed overnight at 4°C with 1C1/3A2 at 0.5 μg/μL in blocking solution, incubated with Cy2-labeled goat anti-mouse (Amersham Biosciences) for 2 hours at room temperature in blocking buffer, extensively washed, coverslipped with mounting medium (Vector Laboratories), and viewed under a fluorescence microscope (Olympus BX50). Image analysis was performed as described subsequently. For the detection and relative quantification of ERK2, Phospho-ERK1/2, actin, and IDE by Western blot astrocytes were plated onto 24-wells plates at density of 8 $\times$ 10^5 cells/well and treated as described previously. After treatment, medium was removed and stored for cytokines quantification using commercially available kits (BD optEIA; Pharmingen, San Diego, CA) and cells lysed in 100 μL of Laemmli sample buffer and aliquots (previously normalized by protein content) processed for immunoblots as previously described.

Image and Statistical Analysis

Immunostained brain sections were imaged with a digital Olympus BX50 microscope, and assessment of levels of Aβ burden and IDE/GFAP immunoreactivity was performed using the Image-Pro Plus software (Media Cybernetics). Additional analysis of double-labeled sections was performed by laser scanning confocal microscopy imaging sections on LSM5 Pascal microscope using a 3-frame filter and Zeiss LSM5 image examiner. For each case, a total of 6 brain sections (10 images per section) were analyzed to estimate the average number of immunolabeled cells per unit area (millimeters squared) and the average intensity of immunostaining (corrected optical density). To quantify the intensity of the fluorescence (corrected optical density) per unit area (millimeters squared) after Aβ treatments, images of at least 100 immunocytochemically stained cells were analyzed by Image-Pro Plus software (Media Cybernetics). Quantitative data were analyzed by one-way analysis of variance with a post hoc Tukey test or 2-tailed Student *t*-test to compare NTg and Tg2576 mice or Aβ treated and untreated cells were performed using GraphPad Prism 3.0 software. All results were represented as means ± standard error of mean. p values lower than 0.05 were considered statistically significant.

RESULTS

Insulin-Degrading Enzyme Is Overexpressed in Aged Tg2576 Brains in Synchrony With Aβ Accumulation

To determine whether APPsw overexpression and sustained Aβ overproduction affect the regulation of endogenous IDE levels in vivo and if these parameters are modulated by aging, we examined brain tissue from Tg2576 mice and NTg littermates aged 4.5 months to 16 months. Toward this aim, specific anti-IDE monoclonal antibodies

1C1 and 3A2 were generated against a rIDE. Both monoclonal antibodies recognized linear epitopes within positions 262 to 530 of rat IDE sequence. Moreover, 1C1 and 3A2 were able to detect endogenous IDE by Western blot and specifically immunoprecipitated a full-length 115 kDa IDE from mouse brain that was recognized by polyclonal BC2 (not shown). As previously described, these antibodies were used to develop a sandwich ELISA assay using recombinant rat IDE (rIDE) as a standard (30). IDE protein levels detected by ELISA in water-soluble brain fractions from all experimental groups analyzed is depicted in Figure 1A. In Tg2576 mice (closed squares), there were no substantial changes in protein IDE levels up to 11 months. However, a significant 2-fold increase (*, $p < 0.05$) was observed at 16 months as compared with 11-month-old animals (612 ± 54.3 ng/mg vs 291.96 ± 23.7 ng/mg, respectively). IDE amounts in 16-month-old Tg2576 animals were statistically different from all control samples analyzed (*, $p < 0.05$). No differences in IDE levels were observed among mice from the NTg groups (closed triangles), suggesting that steady-state levels of the IDE protein are not significantly modulated by aging in these animals. We next tested Aβ40 and Aβ42 in PBS and SDS-soluble brain fractions, respectively. As previously reported (34), as Tg2576 animals age, Aβ40 and Aβ42 (not shown) accumulate progressively with the former reaching the highest levels at 16 months of age. Aβ40 was more abundant than Aβ42 and both species were highly enriched in the SDS preparations as compared with water-soluble homogenates (not shown). Notably, the sharp increase in the amount of IDE (closed squares) in 16-month-old Tg2576 mice correlated with the exponential rise of SDS-soluble Aβ40 accumulation (opened circles) (Fig. 1B). To confirm that the increase in IDE levels observed by ELISA in 16-month-old Tg2576 animals was the result of the full-length protease and not proteolytic fragments, we performed Western blots of water-soluble and SDS-soluble brain homogenates from all the mice involved in the study. The polyclonal antibody BC2 revealed that 115 kDa IDE was significantly increased in the brain of 16- as compared with 11-month-old Tg2576 mice (Fig. 1C), whereas no differences were observed among NTg animals (not shown). When normalized to corresponding neuronal specific enolase (NSE) immunoreactivity, water-soluble IDE levels of Tg2576 mice at 16 months of age were on average almost 3-fold higher as compared with 1-month-old Tg2576 mice (0.715 ± 0.115 arbitrary units [AU] vs 0.255 ± 0.025 AU, **, $p < 0.01$) (Fig. 1C). These results were fully consistent with the ELISA data and confirmed that IDE is increased at the time when brain Aβ species approached their highest levels. Subcellular localization experiments have shown that IDE is mainly located in the cytosol; however, it is also present in membrane fractions that may be more relevant to Aβ degradation (14, 34–36). Therefore, we were interested in determining the levels of IDE present in water-insoluble compartments. The pellets obtained in PBS were exhaustively washed in carbonate buffer pH 11 to eliminate weak associations with integral membrane proteins and further treated with 2% SDS. For loading controls and normalization, membranes were reprobed with antibodies antiflotillin, a raft-associated protein (37). In agreement with the results

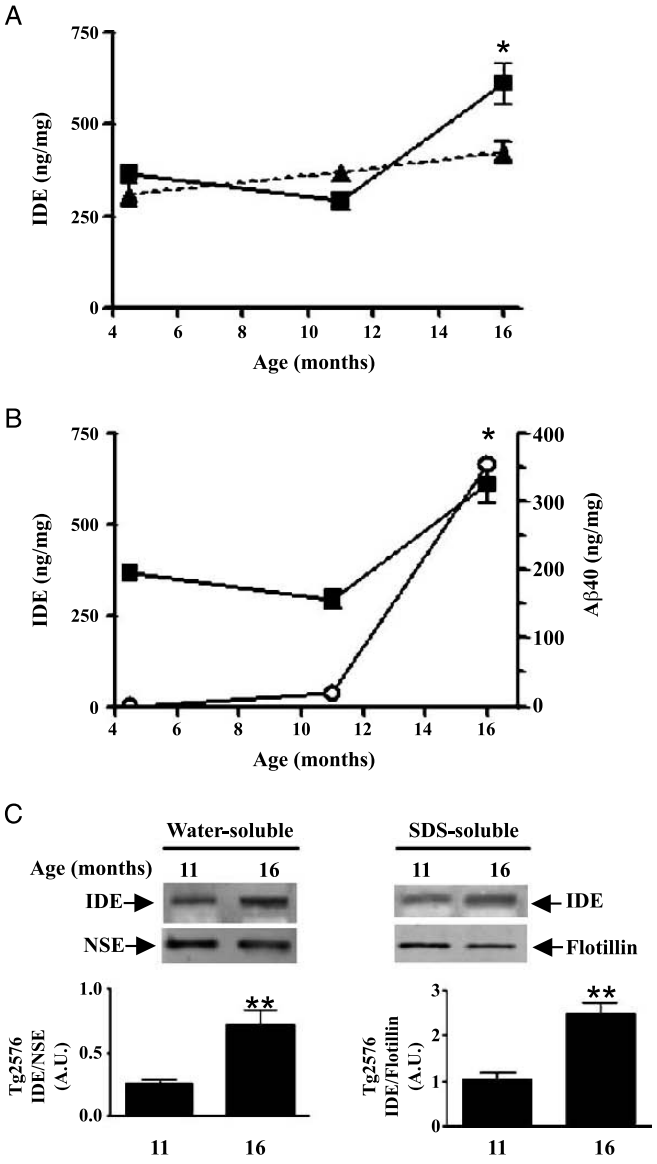

FIGURE 1. Insulin-degrading enzyme (IDE) and Aβ levels in aging Tg2576 brain. **(A)** IDE levels in water-soluble homogenates of Tg2576 (closed squares) and NTg (closed triangles) mice. **(B)** Amount of Aβ40 (opened circles) and IDE (closed squares) in Tg2576 animals. Aβ determinations were performed in 2% SDS-soluble brain homogenates. *, $p < 0.05$ as compared with 11-month-old Tg2576 and NTg animals. **(C)** Western blots of water-soluble and SDS-soluble homogenates of Tg2576 mice probed on the same membrane with anti-IDE BC2, anti-NSE, and antiflotillin, respectively. The graphs show IDE levels in arbitrary units (AU), normalized by anti-NSE and antiflotillin immunoreactivity. Data represent the mean ± standard error of mean of 4 experiments with at least 4 animals in each group. **, $p < 0.01$ as compared with 11-month-old Tg2576.

obtained with the water-soluble fractions, a significant 2-fold increment of IDE in SDS-soluble fraction from 16-month-old as compared with 11-month-old animals was found (2.495 ± 0.22 vs 1.03 ± 0.129, **, $p < 0.01$) (Fig. 1C).

Insulin-Degrading Enzyme Activity in Brain Homogenates From Young and Aged Tg2576 Mice

To evaluate if the higher levels of IDE detected in aged mice were reflected in its proteolytic activity, we used a test based on the immunoprecipitation of PBS-soluble proteins from mouse brain homogenates with both anti-IDE monoclonal antibodies (1C1 and 3A2) using ^{125}I-insulin as a substrate as previously described (30). A representative SDS-PAGE and PhosphorImager analysis of ^{125}I-insulin degradation by Tg2576 and NTg animals of 11 and 16 months, respectively, and rIDE is shown in Figure 2. Degraded fractions of 30.3 ± 7.8% and 56.2 ± 16.1% of ^{125}I-insulin by Tg2576 of 11 and 16 months, respectively, were observed as compared with the 100% defined for rIDE-positive control. Moreover, no differences in proteolytic activity were observed between 11- and 16-month-old NTg mice (degraded fractions of 27.6 ± 2.23% and 26.8 ± 2.2% of ^{125}I-insulin, respectively). Our results showed a 1.8-fold increase in the mean value of the enzyme activity in aged as compared with younger Tg2576 mice, which positively correlated with the 2-fold increase in the amount of IDE protein level. It is important to notice that these values did not reach statistical significance as a result of large standard errors of the mean, and therefore we cannot rule out that part of the total amount of immunoprecipitated IDE in aged Tg2576 mice may be inactive.

The Amount of Insulin-Degrading Enzyme mRNA Is the Same in Brain Homogenates From Young and Aged Tg2576 Mice

To evaluate if the increment of IDE observed in aged Tg2576 animals was associated with transcriptional upregulation of IDE mRNA, competitive RT-PCR was performed in brain tissue from 11 and 16 months animals normalized by GPDH (Fig. 3A). Representative gels with the calibration curve performed with competitor mRNA to determine the levels of endogenous IDE mRNA from 11 and 16 months samples are shown in Figure 3B (left panel). No significant differences were detected in the amount of IDE transcripts in whole brain homogenates from 11- and 16-month-old Tg2576 mice (Fig. 3B, right panel) as well as compared with 16-month-old NTg mice (not shown). Our results indicate that IDE increment detected in aged Tg2576 mice was not the result of a widespread increase in its mRNA levels and suggest that regulation of IDE in aged mice may occur at the posttranscriptional level. Alternatively, a localized overexpression may not be reflected in total brain mRNA.

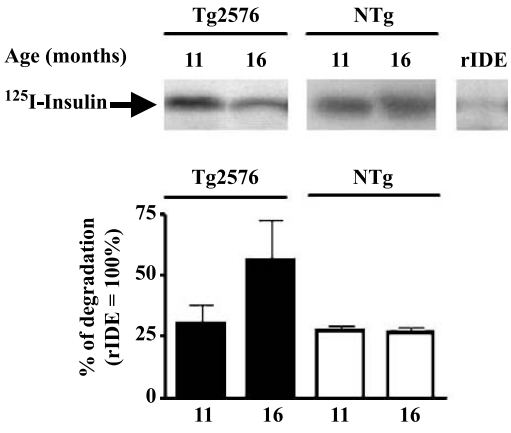

FIGURE 2. Activity of insulin-degrading enzyme (IDE) in water-soluble brain homogenates of aging Tg2576 and NTg animals. Representative PhosphorImage scans showing the degradation of ^{125}I-insulin after incubation with anti-IDE (1C1 and 3A2) immunoprecipitates from samples of 11- and 16-month-old Tg2576 and NTg mice, and rIDE, respectively. The graph shows the densitometric quantitation of the endogenous IDE activity shown in the upper panel. Bars represent the mean ± standard error of mean of 3 independent experiments.

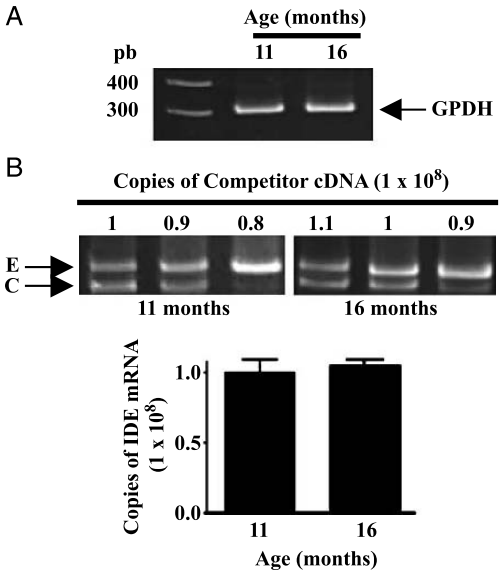

FIGURE 3. Age-related changes in insulin-degrading enzyme (IDE) mRNA in brains from transgenic Tg2576 mice as revealed by competitive reverse transcriptase–polymerase chain reaction (RT-PCR). **(A)** Normalization of total brain mRNA from 11- and 16-month-old Tg2576 mice by GPDH content. **(B)** Representative gel of RT-PCR products from endogenous IDE mRNA from 11- and 16-month-old animals with increasing competitor RNA amounts. The graph shows the number of copies of endogenous IDE transcripts from 11- and 16-month-old Tg2576 mice. Bars represent the mean ± standard error of mean of 3 independent experiments.

The Intensity of Astroglial Activation Correlates With Insulin-Degrading Enzyme Overexpression in Tg2576Mice

To test whether late inflammatory foci would be accompanied by IDE expression, quantitative Western blotting and immunohistochemistry of the astrocytic-specific marker GFAP were performed. There was a sharp increase in GFAP levels from brain homogenates at 16-month-old as compared with 11-month-old Tg2576 (3.66 ± 0.15 AU and 1.63 ± 0.05 AU, respectively) (*, $p < 0.05$), which

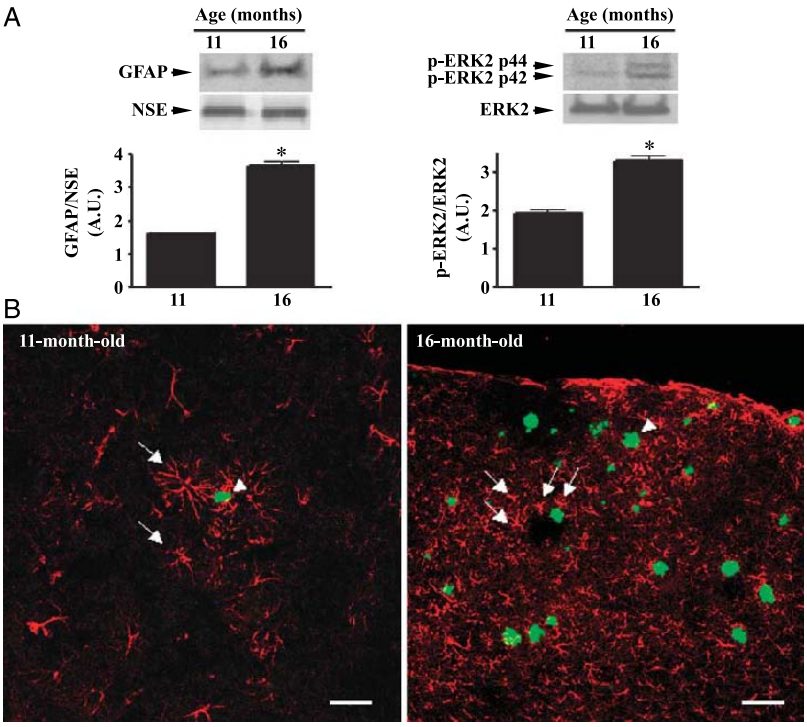

FIGURE 4. GFAP levels and ERK1/2 activation in aging Tg2576 brain. **(A)** Western blots of water-soluble homogenates of 11- and 16-month-old Tg2576 mice probed on the same membrane with anti-GFAP and anti-NSE or anti-ERK2 and anti-p-ERK1/2, respectively. The graph shows GFAP and p-ERK1/2 levels in arbitrary units (AU), normalized by NSE and ERK2 immunoreactivity, respectively. Data represent the mean ± standard error of mean of 3 experiments with at least 4 animals in each group. *, $p < 0.05$ as compared with 11-month-old Tg2576. **(B)** Pictures show thioflavin-S reactive amyloid plaques (green, arrowheads) and peripheral GFAP-positive astrocytes (red, arrows) distributed along the cortex of coronal brain sections from 11- and 16-month-old Tg2576 mice. Scale bar = 50 μm.

correlated with the upregulation of the p-ERK1/2 kinase (3.29 ± 0.12 AU and 1.93 ± 0.092 AU, respectively) (*, $p < 0.05$) and a widespread activation of astrocytes associated to deposited Aβ in the hippocampus, brain cortices (visual, auditory, entorhinal, and piriform), and amygdaloid nuclei of the affected brain (Fig. 4). In our study, plaques were detected at 11 months of age in agreement with the quantitative ELISA data of Aβ levels. Although a cytoplasmic label homogenously distributed along neurons from all regions of the brain was seen, IDE overexpression (black) was related to cells in the vicinity of plaques in 11- (Fig. 5A) and 16-month-old Tg2576 mice as well as in the outer rim of the thioflavin-S positive deposits (yellow) (Fig. 5B). This localized IDE staining was not found in NTg mice of all ages analyzed, although a cytoplasmic neuronal staining similar to Tg2576 mice was detected (not shown). To further explore whether IDE immunoreactivity surrounding Aβ plaques overlapped with glial cells, labeling with anti-GFAP (red, astrocytes) or FITC-tomato lectin (green, microglia) and 1C1/3A2 (purple, anti-IDE) was performed. We observed that 15 ± 7% and 61 ± 10% of GFAP-immunoreactive astrocytes in the vicinity of plaques were strongly positive for IDE (purple) in 11- and 16-month-old Tg2576 mice, respectively (Fig. 5C–E), in accordance with the increments observed by ELISA and Western blot. By contrast, well-defined fluorescent (green) microglial cell bodies surrounding amyloid plaques (Fig. 5F) lacked IDE immunoreactivity (Fig. 5G). Merging of both images (Fig. 5H) ruled out microglial–IDE overproduction and suggests that the rim of IDE staining at the plaque periphery (Fig. 5B) may be the result of dystrophic neurites (38, 39).

Fibrillar Aβ Induces Insulin-Degrading Enzyme Upregulation in Astrocyte Through the Activation of Mitogen-Activated Protein Kinase Cascade

To explore a potential mechanism by which IDE is upregulated surrounding plaques in aged Tg2576 mice, we conducted in vitro experiments in primary astrocytes cultures exposed to 5 μM soluble or fibrillar Aβ (sequences 1–40) (Fig. 6A). A significant 1.75-fold increment was observed by Western blot in IDE after treatment with fibrillar peptide as compared with control cultures (treated with 5% DMSO) (30.4 ± 3.75 AU vs 17.3 ± 2.04 AU, *, $p < 0.05$), and no differences were detected when soluble Aβ was used (20.37 ± 2.57 vs 25.14 ± 2.02 AU) (Fig. 6B). These data were further supported by immunocytochemistry results that showed that fibrillar Aβ exposure increased the intensity of cytoplasmic and membrane-associated IDE staining per cell in primary rat astrocytes approximately 40% relative to controls (mean fluorescence [optical density]/mean area [mm^3] = 0.07 AU vs 0.11 AU) (Fig. 6C). At this concentration, no cell loss was detected as measured by a nuclear stain, DAPI (not shown).

Taking into account that Aβ specifically promotes phosphorylation and nuclear translocation of ERK1/2 (40) in cultured rat cortical astrocytes, we decided to explore the involvement of this signaling pathway on IDE expression. Specific inhibition of the ERK1/2 pathway was confirmed by the strong decrease in the levels of p-ERK1/2 after the addition of U0126 (2.3-fold reduction as compared with control) as assessed by Western blot without alteration on ERK2 and actin levels (Fig. 7A). Under these experimental

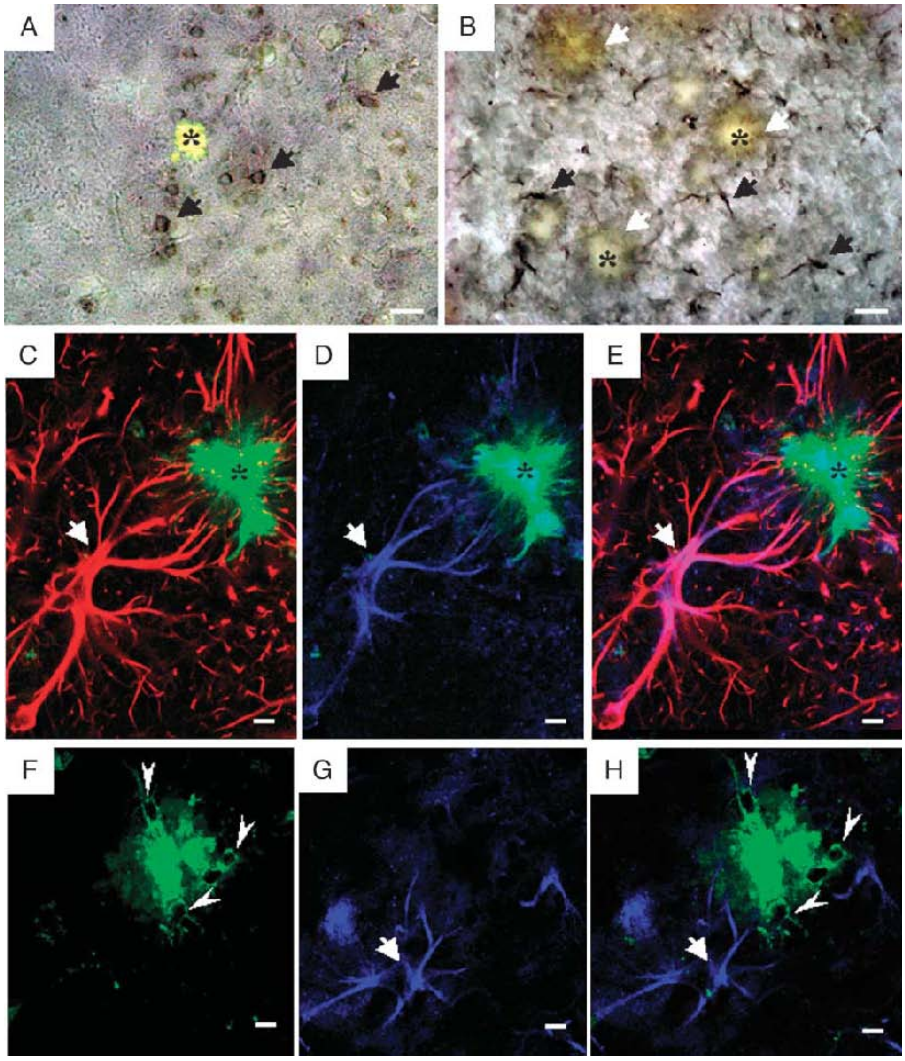

FIGURE 5. Plaque-associated insulin-degrading enzyme (IDE) overexpression. Representative immunohistochemistry images of IDE expression (black staining) in brain sections from **(A)** 11-month-old and **(B)** 16-month-old Tg2576 mice. Note the cytoplasmic IDE labeling (black arrows) in 11- and 16-month-old Tg2576 mice and IDE immunoreactivity (white arrows) around fibrillar amyloid (asterisk) only in old mice. Confocal microscopy analysis shows that the same GFAP-immunoreactive astrocyte (**[C]**, red) that is next to the thioflavin-S-reactive plaque (green) is positive for IDE (**[D]**, blue) as represented in the merged (purple) image **(E)**. Double labeling with FITC–tomato–lectin shows that activated microglial cells (**[F]**, arrowheads) surrounding amyloid deposits are negative for IDE (**[G]**, arrows) as represented in the merged image **(H)**. Asterisk indicates an amyloid plaque. Scale bars = **(A, B)** 50 μm; **(C–H)** 10 μm. *a+*

conditions, the observed stimulation of IDE expression after fibrillar Aβ exposure was approximately 30% as compared with DMSO or reverse peptide Aβ (sequences 40–1)-treated cells. Overexpression of IDE by fibrillar Aβ was reverted by U0126 (Fig. 7B) confirming the involvement of ERK1/2 cascade on IDE expression.

DISCUSSION

The mechanisms by which IDE mRNA and protein steady-state levels are regulated in the brain are poorly understood. In this study, we used both in vivo and in vitro strategies to explore the association between IDE levels and Aβ accumulation. We found that IDE, a key protease involved in the clearance of Aβ from the brain, is overexpressed in an active form by glial cells in aged Tg2576 mice (16 months). It was previously reported that the Aβ burden in these mice increases over their lifespan (16–17 months) and the plaque generation time in this animal model has been estimated to be approximately 1 year. Moreover, aging is not associated in Tg2576 with an increase of β-secretase activity (41), and the augmented production of Aβ is not sufficient to induce amyloid deposition at early ages. The positive correlation between measurements of IDE protein and its activity suggests that the increased IDE levels in aged Tg2576 were not a compensation for reduced activity of the enzyme and support the notion that in this animal model, IDE activity is unaffected by aging. Our finding of similar IDE levels in NTg and Tg2576 mice up to 11 months is in agreement with a recent report in which IDE was detected by Western blot in 5- and 14-month-old NTg and Tg2576 brain homogenates using BC2 anti-IDE polyclonal antibody (42). By contrast, reduction in IDE expression in aged mice was reported using different anti-IDE polyclonal antibodies and different animal models of AD (43, 44). The variability in the pattern of expression and activity of endogenous IDE from various transgenic mice models of AD may be the consequence of differences in their genetic backgrounds and/or in the specificity of anti-IDE antibodies used.

Competitive RT-PCR did not show significant differences between the amounts of IDE transcripts in whole brain homogenates from 11- and 16-month-old animals despite the

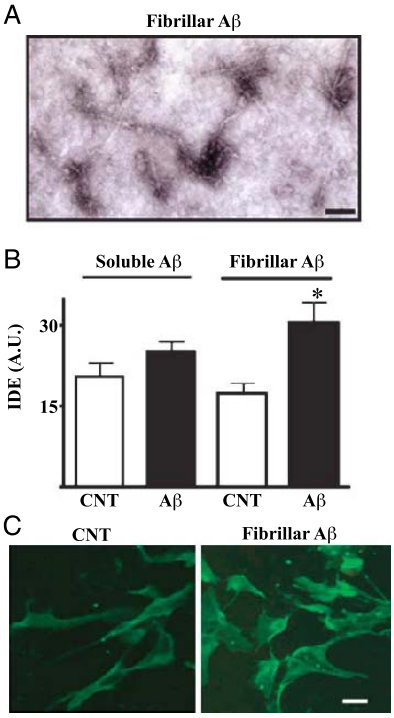

FIGURE 6. Fibrillar Aβ induces insulin-degrading enzyme (IDE) upregulation in primary rat cortical astrocytes. **(A)** Fibrillar Aβ (sequences 1–40) stained with 0.5% of uranyl acetate and viewed under electron microscopy. **(B)** The graph shows IDE levels in arbitrary units (AU) from Western blots of primary rat astrocytes treated with 5% DMSO (control [CNT]), 5 μM soluble, and fibrillar Aβ (sequences 1–40), respectively, solubilized in Laemmli sample buffer, probed with BC2 anti-IDE polyclonal antibody, and normalized by protein content (not shown). Data represent the mean ± standard error of mean of 3 experiments. *, $p < 0.05$ relative to CNT. **(C)** Immunocytochemical images showing fibrillar Aβ (sequences 1–40)-induced IDE upregulation on in vitro primary rat astrocytes treated as described previously and followed by determination of IDE by immunocytochemical staining using 1C1/3A2 anti-IDE monoclonal antibodies. Scale bars = **(A)** 100 nm; **(C)** 10 μm.

protein increment observed, suggesting that during this temporal window, the global rate of IDE transcription does not change. These data are in agreement with the reported changes of Neprilysin mRNA expression in this animal model (45). The lack of a positive correlation between the total IDE mRNA and protein raises the possibility that IDE is regulated at a posttranscriptional level, including increased stability of mRNA or decreased protein turnover rate resulting from age-related modifications. The former possibility could be experimentally addressed by in vitro experiments exposing cell cultures to TGF-β_1, a known inductor of APP mRNA stabilization (46). Regarding posttranslational modifications, IDE may be oxidized in the hippocampus of AD brains and this change may render IDE less effective in degrading Aβ (43). Our sandwich ELISA and the immunoprecipitation activity assay are based on monoclonal antibodies that do not recognize posttranslational modifications. Therefore, we were likely detecting total soluble IDE and cannot rule out that a fraction of IDE may be oxidized and inactive in Tg2576 mice.

This is the first report to our knowledge that shows IDE immunoreactivity in Tg2576 brain sections. We demonstrated that in old Tg2576 mice, IDE was distributed along a concentric ring next to dystrophic neurites and in activated astrocytes, suggesting that chronic Aβ deposition in Tg2576 mouse brain may induce a selective IDE overexpression by astrocytes. The highly localized IDE immunoreactivity pattern that we found may also explain

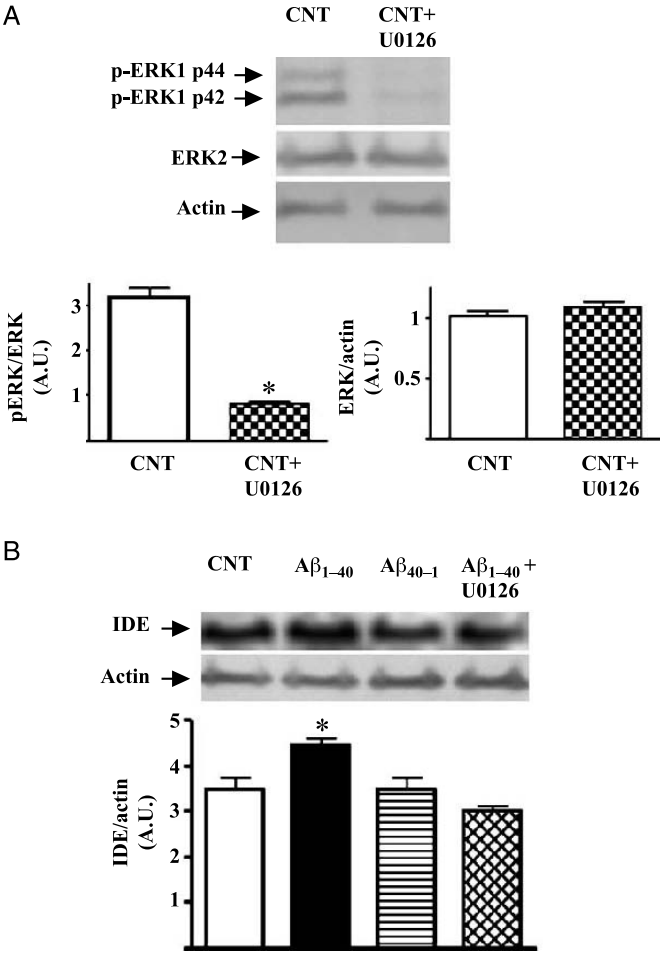

FIGURE 7. Fibrillar Aβ induces insulin-degrading enzyme (IDE) upregulation through ERK2 cascade in primary rat cortical astrocytes. **(A)** Western blots of control (CNT) and U0126 pretreated cells probed on the same membrane with anti-pERK1/2, anti-ERK2, and anti-actin. The graphs show pERK1/2 and ERK2 levels in arbitrary units (AU), normalized by ERK2 and actin, respectively. Bars indicate the mean ± standard error of mean of 3 independent experiments (*, $p < 0.05$ relative to CNT). **(B)** Western blots of control (CNT, lane 1) or cells stimulated with 5 μM fibrillar Aβ (lane 2), 5 μM reverse Aβ (lane 3), and U0126 + 5 μM fibrillar Aβ (lane 4), respectively, probed on the same membrane with BC2 and antiactin. The graph shows IDE levels in arbitrary units (AU) normalized by actin. Bars indicate the mean ± standard error of mean of 3 independent experiments (*, $p < 0.05$ relative to U0126).

the discrepancy between whole brain mRNA and IDE protein levels detected. These immunohistochemical data are consistent with the strong increase in GFAP levels observed by Western blot in 16-month-old Tg2576 mice and are in accordance with a previous report indicating that Aβ deposits may induce local astrocyte activation together with upregulation of Neprilysin (45). IDE overexpression associated with Aβ deposition in Tg2576 may be highly sensitive to pathologic changes in the environment of glial cells. It was previously reported (47) that the recruitment of glial cells in Tg2576 mice is a rather slow process. In our study, the presence of IDE in reactive astrocytes and surrounding amyloid deposits at 16 months of age was always associated with the confluence of small amyloid cores, reinforcing that the accumulation of IDE depends on plaque age rather than on the sole presence or size of fibrillar amyloid cores. The lack of IDE overexpression by microglial cells may be explained by the different responses of each cell type for each chemokine produced in different phases during acute or chronic inflammation as recently proposed (48). In this regard, protein kinase C (PKC), mainly involved in MAPK/ERK cascade, was reported to be less expressed in microglia as compared with astrocytes, suggesting that different patterns of expression of PKC in the 2 cell types (49) contribute to the differences in the ability of specific stimuli to enhance responses in astrocytes but not in microglia. At the present stage of our investigation, however, we can only speculate whether the low percentage of GFAP-immunoreactive astrocytes positive for IDE observed in young Tg2576 brain indicates the lack at this age of the specific stimuli or an inhibition of astroglial IDE expression. Noteworthy, enzymatically active IDE accumulation in Tg2576 mice brain does not correlate with the observations by our group and others that were obtained from cortex and hippocampus of patients with AD and in cortical microvessels with amyloid angiopathy (25, 26, 30). Notably, amyloid cores from Tg2576 mice lacked IDE immunoreactivity opposite to a previous report showing colocalization of IDE with amyloid deposits in AD brain (50) but in accordance with a comprehensive proteomic analysis of senile plaques from postmortem AD brain tissues (51). Our results are in agreement with the notion that the profile of inflammatory markers between Tg2576 and human AD brains is different (52), reflecting differences in inflammatory responses triggered by fibrillar Aβ between human and rodents. In this sense, plaque formation in Tg2576 mice may be less influenced by Aβ posttranslational modifications as a result of their shorter generation time as compared with human AD (53). In addition, Aβ levels in Tg2576 mice are relatively much higher than in sporadic AD, and they appear to be sufficient to initiate seed formation and plaque growth without additional factors that may be critical in sporadic AD related to APOE genotype, cholesterol levels, inflammation, and age-related oxidative damage, which may in turn influence IDE regulation.

Our in vitro experiments indicate that fibrillar Aβ, a potent activator of glial cells, promotes IDE expression in astrocytes through ERK 1/2 phosphorylation, reinforcing the notion that IDE may be directly involved in brain inflammatory pathways. It was previously reported that neuronal IDE is a downstream target in the insulin receptor signaling cascade mediated by phosphatidylinositol-3 kinase (PI3K)-Akt phosphorylation (54) and that this pathway is inhibited in primary neuronal cultures by extracellular fibrillar Aβ (55) or by intraneuronal aggregates of Aβ (56). Contradictory experimental evidence involves Aβ in the activation of MAPK cascades, including JNK (57), ERK1/2 (58), and p38 (59). The inhibition of IDE overexpression by fibrillar Aβ on U0126-pretreated primary cortical astrocytes suggests that fibrillar Aβ triggers different signaling cascades that target IDE expression. Moreover, IDE overexpression resulting from ERK1/2 activation by fibrillar Aβ in vivo and in vitro may explain the reduction of diffuse Aβ loads in Tg2576 mice (60). The lack of detection of p-p38 by fibrillar Aβ (not shown) in primary rat astrocytes is in agreement with a previous report, suggesting that this kinase is not functional in cultured rat cortical astrocytes (40). Remarkably, after Aβ treatment, levels of IL-1β and IL-6 in the supernatant were undetectable (not shown), probably as a result of the low sensitivity of the capture ELISA assay used or a lack of response of primary rodent astrocytes to secrete these inflammatory cytokines after Aβ stimulation. Our results suggest that ERK1/2 is an upstream signaling pathway contributing to IDE upregulation by fibrillar Aβ in astrocytes pointing to a causal relationship between an inflammatory cascade and IDE expression. Notably, the pattern of IDE expression that we report at different ages in Tg2576 is in agreement with the profile of IL-1β, TGF-β, IL-6, and IL-10-positive astrocytes (61) and advanced glycation end products (AGEs) immunoreactivity (62), previously described. The novo synthesis inside activated glial cells from aged Tg2576 mice of IL-6, IL-10, and AGEs was proposed by different authors as a protective mechanism developed during lifespan in this animal model of AD. In this context, because IDE is unable to degrade aggregated amyloid peptides (29), a sustained overexpression of IDE by astrocytes in Tg2576 at late stages of neuropathologic alterations may be interpreted as part of a late reaction triggered by fibrillar Aβ toward degrading soluble Aβ peptides to limit plaque growth and its associated disruption of synaptic circuits (63). Alternatively, it may be a defensive strategy aimed to protect neurons from death by functions still unexplored for IDE such as the inhibition of apoptosis or promotion of cell survival—hypotheses that could be experimentally tested.

REFERENCES

1. Glenner GG. The pathobiology of Alzheimer's disease. Annu Rev Med 1989;40:45–51
2. Poirier J. Apolipoprotein E, cholesterol transport and synthesis in sporadic Alzheimer's disease. Neurobiol Aging 2005;26:355–61
3. Wolfe MS. Secretase(s?) as a target for Alzheimer's disease. Curr Top Med Chem 2002;2:371–83
4. Dewachter I, Van Dorpe J, Smeijers L, et al. Aging increased amyloid peptide and caused amyloid plaques in brain of old APP/V717I transgenic mice by a different mechanism than mutant presenilin 1. J Neurosci 2000;20:6452–58
5. Shibata M, Yamada S, Kumar SR, et al. Clearance of Alzheimer's amyloid-β (1–40) peptide from brain by LDL receptor-related protein-1 at the blood–brain barrier. J Clin Invest 2000;106:1489–99

6. Fakharai-Rad H, Nikoshkov A, Kamel A, et al. Insulin-degrading enzyme identified as a candidate diabetes susceptibility gene in GK rats. Hum Mol Genet 2000;9:2149–58
7. Miller BC, Eckman EA, Sambamurti K, et al. Amyloid-β peptide levels in brain are inversely correlated with insulysin activity levels in vivo. Proc Natl Acad Sci U S A 2003;100:6221–26
8. Farris W, Mansourian S, Chang Y, et al. Insulin-degrading enzyme regulates the levels of insulin, amyloid β-protein, and the β-amyloid precursor protein intracellular domain in vivo. Proc Natl Acad Sci U S A 2003;100:4162–67
9. Farris W, Mansourian S, Leissring MA, et al. Partial loss-of-function mutations in insulin-degrading enzyme that induce diabetes also impair degradation of amyloid β-protein. Am J Pathol 2004;164:1425–34
10. Morelli L, Bulloj A, Leal MC, et al. Amyloid beta degradation: A challenging task for brain peptidases. Subcell Biochem 2005;38:129–45
11. Marr RA, Rockenstein E, Mukherjee A, et al. Neprilysin gene transfer reduces human amyloid pathology in transgenic mice. J Neurosci 2003; 23:1992–96
12. Leissring MA, Farris W, Chang AW, et al. Enhanced proteolysis of β-amyloid in APP transgenic mice prevents plaque formation, secondary pathology, and premature death. Neuron 2003;40:1087–93
13. Rawlings ND, Tolle DP, Barret AJ. MEROPS: The peptidase database. Nucleic Acids Res 2004;32:D160–64
14. Becker AB, Roth RA. An unusual active site identified in a family of zinc metalloendopeptidases. Proc Natl Acad Sci U S A 1992;89: 3835–39
15. Morelli L, Llovera R, Ibendahl S, et al. The degradation of amyloid β as a therapeutic strategy in Alzheimer's disease and cerebrovascular amyloidoses. Neurochem Res 2002;21:1387–99
16. Morelli L, Llovera RE, Alonso LG, et al. Insulin-degrading enzyme degrades amyloid peptides associated with British and Danish familial dementia. Biochem Biophys Res Commun 2005;332:806–14
17. Groves CJ, Wiltshire S, Smedley D, et al. Association and haplotype analysis of the insulin-degrading enzyme (IDE) gene, a strong positional and biological candidate for type 2 diabetes susceptibility. Diabetes 2003;52:1300–305
18. Karamohamed S, Demissi S, Volcjak J, et al. Polymorphisms in the insulin-degrading enzyme gene are associated with type 2 diabetes in men from the NHLBI Framingham Heart Study. Diabetes 2003;52:1562–67
19. Bertram L, Blacker D, Mullin K, et al. Evidence for genetic linkage of Alzheimer's disease to chromosome 10q. Science 2000;290:2302–303
20. Abraham R, Myers A, Wavrant-DeVrieze F, et al. Substantial linkage disequilibrium across the insulin-degrading enzyme locus but no association with late-onset Alzheimer's disease. Hum Genet 2001;109: 646–52
21. Blomqvist ME, Chalmers K, Andreasen N, et al. Sequence variants of IDE are associated with the extent of β-amyloid deposition in the Alzheimer's disease brain. Neurobiol Aging 2005;26:795–802
22. Feuk L, McCarthy S, Andersson B, et al. Mutation screening of a haplotype block around the insulin degrading enzyme gene and association with Alzheimer's disease. Am J Med Genet B Neuropsychiatr Genet 2005;136B:69–71
23. Bian L, Yang JD, Guo TW, et al. Insulin-degrading enzyme and Alzheimer disease: A genetic association study in the Han Chinese. Neurology 2004;63:241–45
24. Nowotny P, Hinrichs AL, Smemo S, et al. Association studies between risk for late-onset Alzheimer's disease and variants in insulin-degrading enzyme. Am J Med Genet B Neuropsychiatr Genet 2005;136B:62–68
25. Perez A, Morelli L, Cresto JC, et al. Degradation of soluble amyloid beta-peptides 1–40, 1–42, and the Dutch variant 1-40Q by insulin degrading enzyme from Alzheimer disease and control brains. Neurochem Res 2000;25:247–55
26. Cook DG, Leverenz JB, McMillan PJ, et al. Reduced hippocampal insulin-degrading enzyme in late-onset Alzheimer's disease is associated with the apolipoprotein E-epsilon4 allele. Am J Pathol 2003;162: 313–19
27. Hsiao K, Chapman P, Nilsen S, et al. Correlative memory deficits, Aβ elevation, and amyloid plaques in transgenic mice. Science 1996;274: 99–102
28. Sigurdsson EM, Lorens SA, Hejna MJ, et al. Local and distant histopathological effects of unilateral Aβ 25-35 injections into the amygdala of young F344 rats. Neurobiol Aging 1996;17:893–901
29. Morelli L, Llovera R, Gonzalez SA, et al. Differential degradation of amyloid β genetic variants associated with hereditary dementia or stroke by insulin-degrading enzyme. J Biol Chem 2003;278:23221–26
30. Morell L, Llovera RE, Mathov I, et al. Insulin-degrading enzyme in brain microvessels: Proteolysis of amyloid β vasculotropic variants and reduced activity in cerebral amyloid angiopathy. J Biol Chem 2004;279: 56004–13
31. Santos J, Gebhard LG, Risso VA, et al. Folding of an abridged beta-lactamase. Biochemistry 2004;43:1715–23
32. Pasquini LA, Paez PM, Moreno MA, et al. Inhibition of the proteasome by lactacystin enhances oligodendroglial cell differentiation. J Neurosci 2003;23:4635–44
33. Srinivasan R, Jones EM, Liu K, et al. pH-dependent amyloid and protofibril formation by the ABri peptide of familial British dementia. J Mol Biol 2003;333:1003–23
34. Thinakaran G, Teplow DB, Siman R, et al. Metabolism of the 'Swedish' amyloid precursor protein variant in neuro2a (N2a) cells. Evidence that cleavage at the 'beta-secretase' site occurs in the Golgi apparatus. J Biol Chem 1996;271:9390–97
35. Vekrellis K, Ye Z, Qiu WQ, et al. Neurons regulate extracellular levels of amyloid beta-protein via proteolysis by insulin-degrading enzyme. J Neurosci 2000;20:1657–65
36. Gasparini L, Gouras GK, Wang R, et al. Stimulation of beta-amyloid precursor protein trafficking by insulin reduces intraneuronal beta-amyloid and requires mitogen-activated protein kinase signaling. J Neurosci 2001;21:2561–70
37. de Gassart A, Geminard C, Fevrier B, et al. Lipid raft-associated protein sorting in exosomes. Blood 2003;102:4336–44
38. Geddes JW, Anderson KJ, Cotman CW. Senile plaques as aberrant sprout-stimulating structures. Exp Neurol 1986;94:767–76
39. Ard MD, Cole GM, Wei J, et al. Scavenging of Alzheimer's amyloid beta-protein by microglia in culture. J Neurosci Res 1996;43:190–202
40. Abe K, Hisatomi R, Misawa M. Amyloid β peptide specifically promotes phosphorylation and nuclear translocation of the extracellular signal-regulated kinase in cultured rat cortical astrocytes. J Pharmacol Sci 2003;93:272–78
41. Apelt J, Bigl M, Wunderlich P, et al. Aging-related increase in oxidative stress correlates with developmental pattern of beta-secretase activity and beta-amyloid plaque formation in transgenic Tg2576 mice with Alzheimer-like pathology. Int J Dev Neurosci 2004; 22:475–84
42. Yamamoto M, Horiba M, Buescher JL, et al. Overexpression of monocyte chemotactic protein-1/CCL2 in beta-amyloid precursor protein transgenic mice show accelerated diffuse beta-amyloid deposition. Am J Pathol 2005;166:1475–85
43. Caccamo A, Oddo S, Sugarman MC, et al. Age-and region-dependent alterations in A-beta-degrading enzymes: Implications for A-beta-induced disorders. Neurobiol Aging 2005;26:645–54
44. Hwang DY, Cho JS, Kim CK, et al. Aging-related correlation of insulin-degrading enzyme with β-secretase-generated products involving insulin and glucose levels in transgenic mice. Neurochem Res 2005; 30:1171–77
45. Apelt J, Ach K, Schliebs R. Aging-related down-regulation of neprilysin, a putative beta-amyloid-degrading enzyme, in transgenic Tg2576 Alzheimer-like mouse brain is accompanied by an astroglial upregulation in the vicinity of beta-amyloid plaques. Neurosci Lett 2003;339:183–86
46. Amara F, Junaid A, Clough RR, et al. TGF-beta(1), regulation of alzheimer amyloid precursor protein mRNA expression in a normal human astrocyte cell line: mRNA stabilization. Mol Brain Res 1999;71: 42–49
47. Wegiel J, Wang KC, Imaki H, et al. The role of microglial cells and astrocytes in fibrillar plaque evolution in transgenic APP(SW) mice. Neurobiol Aging 2001;22:49–61
48. Flynn G, Maru S, Loughlin J, et al. Regulation of chemokine receptor expression in human microglia and astrocytes. J Neuroimmunol 2003; 136:84–93
49. Slepko N, Patrizio M, Levi G. Expression and translocation of protein kinase C isoforms in rat microglial and astroglial cultures. J Neurosci Res 1999;57:33–38
50. Bernstein HG, Ansorge S, Riederer P, Reiser M, Frolich L, Bogerts B. Insulin-degrading enzyme in the Alzheimer's disease brain: Prominent

localization in neurons and senile plaques. Neurosci Lett 1999;263: 161–64
51. Liao L, Cheng D, Wang J, et al. Proteomic characterization of postmortem amyloid plaques isolated by laser capture microdissection. J Biol Chem 2004;279:37061–68
52. Munch G, Apelt J, Kientsch-Engel R, et al. Advanced glycation endproducts and pro-inflammatory cytokines in transgenic Tg2576 mice with amyloid plaque pathology. J Neurochem 2003;86:283–89
53. Kalback W, Watson MD, Kokjohn TA, et al. APP transgenic mice Tg2576 accumulate A beta peptides that are distinct from the chemically modified and insoluble peptides deposited in Alzheimer's disease senile plaques. Biochemistry 2002;22:922–28
54. Zhao L, Teter B, Lim GP, et al. Insulin-degrading enzyme as a downstream target of insulin receptor signaling cascade: Implications for Alzheimer's disease intervention. J Neurosci 2004;24:11120–26
55. Busciglio J, Lorenzo A, Yeh J, et al. Beta-amyloid fibrils induce tau phosphorylation and loss of microtubule binding. Neuron 1995;14: 879–88
56. Magrané J, Rosen KM, Smith RC, et al. Intraneuronal β-amyloid expression downregulates the Akt survival pathway and blunts the stress response. J Neurosci 2005;25:10960–69
57. Troy CM, Rabacchi SA, Hohl JB, et al. β-Amyloid-induced neuronal apoptosis requires c-Jun N-terminal kinase activation. J Neurochem 2001;77:157–64
58. Wei W, Wang X, Kusiak JW. Signaling events in amyloid beta-peptide-induced neuronal death and insulin-like growth factor I protection. J Biol Chem 2002;277:17649–56
59. Daniels WM, Hendricks J, Salie R, et al. The role of the MAP-kinase superfamily in beta-amyloid toxicity. Metab Brain Dis 2001;16:175–85
60. Morgan D, Gordon M, Tan J, et al. Dynamic complexity of the microglial activation response in transgenic models of amyloid deposition: Implications for Alzheimer therapeutics. J Neuropathol Exp Neurol 2005;64:743–53
61. Apelt J, Schliebs R. Beta-amyloid-induced glial expression of both pro-and anti-inflammatory cytokines in cerebral cortex of aged transgenic Tg2576 mice with Alzheimer plaque pathology. Brain Res 2001; 894:21–30
62. Munch G, Apelt J, Rosemarie-Kientsch-Engel, et al. Advanced glycation endproducts and pro-inflammatory cytokines in transgenic Tg2576 mice with amyloid plaque pathology. J Neurochem 2003;86: 283–89
63. Hsia AY, Masliah E, McConlogue L, et al. Plaque-independent disruption of neural circuits in Alzheimer's disease mouse models. Proc Natl Acad Sci U S A 1999;96:3228–33